e-Journal of Nondestructive Testing - ISSN 1435-4934 - www.ndt.net

EWSHM 2024
11th European Workshop on Structural Health Monitoring

Structural Health Monitoring of Aerospace Structures using Guided Electromagnetic Waves in a Dielectric Waveguide at K_a-Band

Manuel E. Rao [1], Vittorio Memmolo [1], Jochen Moll [1], Viktor Krozer [1]

[1] Department of Physics, Goethe University Frankfurt, Germany
rao@physik.uni-frankfurt.de

Abstract. Dielectric waveguide (DW) antenna systems are widely used in millimeter-wave radar applications. A large and innovative field is Structural Health Monitoring (SHM) of aerospace structures. The proposed research aims at detecting structural changes and potential defects at K_a-band on metallic structures that represents the device under test (DUT). To determine the severity of damage compared to the pristine structural state, dimensionless damage indicators (DI) are calculated by the root-mean-square deviation (RMSD) and correlation coefficient deviation (CCD) methods.

The geometric design of the DW is crucial for a barrier-free propagation of guided electromagnetic waves (EWs) of a specific frequency bandwidth inside the dielectric material. In the presented approach, a rectangular DW is designed through numerical modelling which contains a polypropylene (PP) matrix, aluminum walls and two K-connectors, each with an inserted pin. The DW is attached to the surface of a nearly plane DUT connected externally to a vector network analyzer (VNA) that measures the elements of the scattering matrix (S-parameters). The reflection and transmission behavior, reflected in the S-parameters, provide information about the interaction of guided EWs with a damage. It was found that damage sizes of 2 mm can be detected reliably with the proposed methodology. The full paper will present and discuss numerical simulations with CST Microwave Studio with a comparison to experimental measurements.

Keywords: Structural health monitoring, damage detection, rectangular waveguide, dielectric resonator antenna, K_a-band, millimeter-wave sensors, guided electro-magnetic waves, numerical simulation.

1. Introduction

Dielectric waveguides (DWs) are used in a wide range of applications in different frequency bands and geometries [1]. Their strength lies in their flexible scaling, high radiation quality, compatibility with monolithic microwave integrated circuits (MMICs), mechanical simplicity and the possibility of ensuring different radiation patterns when using different

https://doi.org/10.58286/29662

modes [2]. Basic research was carried out to enable optimal propagation of electromagnetic waves (EWs) in the DW when characteristic natural frequencies are reached. By recording measured reflection and transmission parameters, it is possible to theoretically determine the permittivity of the dielectric used in the waveguide [3]. New areas of research have also emerged that are aimed at applicability of DWs.

A large field is structural health monitoring (SHM), in which guided EWs are used to detect damage to test materials non-destructively. In addition to the identification of damage, e.g. on metallic plates [4] or pipes [5], damage can also be localized by determining the propagation time of EWs [6][7]. Metallic boundary conditions are not absolutely necessary for the preservation of signal energy within a waveguide, as the identification of debondings on carbon composites has shown [8]. The damage localization of holes in a laminate was performed with a near-field imaging method in [9] using a DW. The basic information, provided for identification methods, are signal changes between intact and damaged structures [10].

In other works, the focus is on dielectric resonator antennas (DRAs), which simultaneously act as waveguides for the transport of EWs and for efficient radiation. One application involves dividing the DW into several sub-DWs and analyzing the signal outputs [11]. A Y-junction made of flexible, uncladded silicon-based DWs was developed as a passive semiconductor component [12]. It is also possible to transport EWs from one waveguide to another via DWs [13]. The DW is also called dielectric rod antenna, as a rod is inserted into the waveguide behind, but is not necessarily mechanically coupled. In many publications, polyethylene is used as the dielectric. The radiation pattern depends on the tapered end of the DW [14]. The use of an additional dielectric lens serves to focus the radiation and narrow the main lobe in the polar radiation pattern [15]. In [16], an elliptical dielectric lens was formed directly at the end of a flexible DW, which can also be placed on a SiO_2 substrate-bonded patch antenna in MMICs [17]. Another area of application for DWs are 4G and 5G applications [18].

The novelty of this paper is the conception of a DW for damage detection of holes in an aluminum test plate serving as a representative monitoring object, based on the well-known principle of a rectangular cavity resonator with closed metal walls and inserted antennas through connectors. Polypropylene (PP) was chosen as the substrate. Numerical simulations for a two-port were carried out to evaluate the operability in Ka-band. The reliable detectability of damage was tested using damage indicators (DIs), calculated separately using the root means square deviation (RMSD) and correlation coefficient deviation (CCD) methods, and discussed for plausibility. Another new feature is the combination of DIs, each of which is made up of a reflection or transmission parameter.

The remainder of this paper is organized in the following way: Section 2 describes the theoretical background about waveguides in general, the excitation of EWs, two-ports and the damage detection techniques regarding to SHM. Section 3 is about the conception of the DW, the numerical results and the experimental setup in the lab. Section 4 presents the experimental results for damaged and intact structures. Finally, a short summary and an outlook for further research is given in section 5.

2. Theoretical background

2.1 Waveguide theory

Waveguides are used for the low-loss transport of electromagnetic energy in optics and high-frequency technology. They consist of a dielectric material and metallic walls. The dielectric is used for the propagation of excited EWs. The reflection coefficient derived by Fresnel's

equations shows which dielectric is suitable for wave propagation when incident radiation strikes on a boundary surface between two media with different permittivities $\varepsilon_{r,1}$ and $\varepsilon_{r,2}$. In the simplest case, the radiation strikes a non-magnetic boundary area perpendicularly, resulting in a reflection coefficient of

$$R = \left| \frac{\sqrt{\varepsilon_{r,1}} - \sqrt{\varepsilon_{r,2}}}{\sqrt{\varepsilon_{r,1}} + \sqrt{\varepsilon_{r,2}}} \right|^2 . \tag{1}$$

In real conditions, the environment consists of air with $\varepsilon_{r,1} = 1.00059$ (value is taken from CST Microwave Studio). If air is used as the dielectric in the waveguide, the reflection coefficient disappears, i.e. optimum transmission is guaranteed. In this case, the waveguide is also referred as a hollow waveguide. If a dielectric solid is used that has a higher permittivity than air, the waveguide is referred as a DW. For millimeter waves, it is necessary to scale the DW smaller.

Metals are not suitable candidates as dielectrics, as they conduct electric current on the one hand and reflect EWs almost perfectly due to their high permittivity on the other hand. However, they are used as walls for any type of waveguide because they form the necessary metallic boundary conditions for solving Maxwell's equations in three-dimensional space to excite characteristic modes [19].

In electrodynamics, a mode characterizes a propagating EW when the resonant frequency is reached. For rectangular resonators of edge lengths a, b and c along the unit vectors $\hat{\boldsymbol{x}}$, $\hat{\boldsymbol{y}}$ and $\hat{\boldsymbol{z}}$ (see Fig. 1(a)), the cut-off frequencies of the modes are calculated by

$$f_c(m,n,p) = \frac{c_0}{2\sqrt{\varepsilon_r \mu_r}} \sqrt{\left(\frac{m}{a}\right)^2 + \left(\frac{n}{b}\right)^2 + \left(\frac{p}{c}\right)^2}, \qquad a > b > c, \tag{2}$$

where c_0 is the speed of light [20]. For non-magnetic dielectrics, the magnetic permeability μ_r is equal to 1. The integer parameters m, n and p, which result from the periodic boundary conditions of the wave vector, are sorted in descending order relative to the edge length. Only one of the parameters is allowed to be zero.

There are two different types of modes that can be excited in the rectangular resonator: Transverse electric (TE or H) or transverse magnetic (TM or E) modes. In the first case, the electric field vector, and in the second case, the magnetic field vector points perpendicular to the direction of propagation. Transverse electromagnetic (TEM) modes do not exist here, as at least two separate electric conductors must be provided. In the coaxial cable, this requirement is fulfilled [6].

In rectangular resonators, the first mode is the TE_{110} mode. According to equation (2), a smaller cut-off frequency is given with a larger edge length. The mode is characterized by an oscillation belly in the x- and y-directions, which is equal to one half of the wavelength. The amplitude of the wave belly points in the z-direction accordingly. In the quadruple-mode resonator (QMR) of Basavarajappa and Mansour [20], $a = b$ and $c = a/2$ were chosen so that TE_{101}, TE_{011}, TM_{210} and TM_{120} have the same cut-off frequency. The result was a high-quality factor with a narrow bandwidth for the dual TE and TM modes. In addition, a high bandwidth for the single TE_{110} mode is guaranteed for this geometry. The advantage of single mode propagation is that there is no undesirable overlapping of wave crests and troughs, which can have a negative effect on signal quality. At higher frequencies, the adjacent modes are increasingly close together, so that a separation of the modes is no longer possible.

The propagation of EWs in the waveguide can be almost loss-free, if they are perfectly reflected by the metallic walls. To avoid the skin effect, the walls should not be too thin. The skin effect means that the electromagnetic fields (EFs) disappear exponentially due to the high conductivity σ of the metal except for an edge layer. The skin depth

$$\delta = \frac{1}{\sqrt{\pi \mu_0 \sigma f}} \tag{3}$$

is a factor in the exponent that marks the drop to $1/e$ relative to the original field strength. The displacement of EFs inside the conductor is due to Lenz's rule, in which the temporal change of the EFs induces eddy currents on the inner surface of the metallic walls, which counteract their cause [19].

2.2 Excitation of electromagnetic waves

EWs are stimulated via an antenna that is positioned at $\lambda/4$ distances from the walls (see Fig. 1b)). The antenna thus protrudes halfway into the waveguide and enables uniform, spherical radiation of EWs. In the far field, the spherical waves can be approximated as plane waves. The antenna is a metal pin that is connected to the inner conductor of a connector. The outer conductor of the connector is connected to the metal wall of the waveguide. The connector itself is connected to a vector network analyzer (VNA) via a coaxial cable. The connector therefore acts as an adapter for applying EWs from the coaxial cable into the waveguide [21].

EFs are formed within the coaxial cable in such a way that the inner and outer conductors are operated with opposite polarity and thus, electric fields spread out radially from the positively to the negatively charged conductor. Due to Ampère's law for conductors through which current flows with a density, including the term of displacement current, a magnetic vortex field is generated. For transversal EWs, the electric and magnetic field vectors and are perpendicular to each other. In the case of radial electric field lines for TEM modes, the magnetic field lines are therefore concentrically circular to the outer and inner conductor of the coaxial cable (see Fig. 1(c)) [19].

TEM modes can always be excited in the coaxial cable from DC (abbr. for *digital current*, corresponds to 0Hz). It should be noted that the type of connector must be matched to the operating frequency band in the waveguide. TE and TM modes are not desired due to adverse interference with TEM modes [19]. The first mode is the TE_{11} mode, for which the cut-off frequency is estimated as follows:

$$f_{c,\,\mathrm{TE}_{11}} \approx \frac{c_0}{\sqrt{\varepsilon_r \mu_r}\,\pi (R + r)}, \tag{4}$$

where R and r are the radiuses of the outer and inner conductor of the coaxial cable [21].

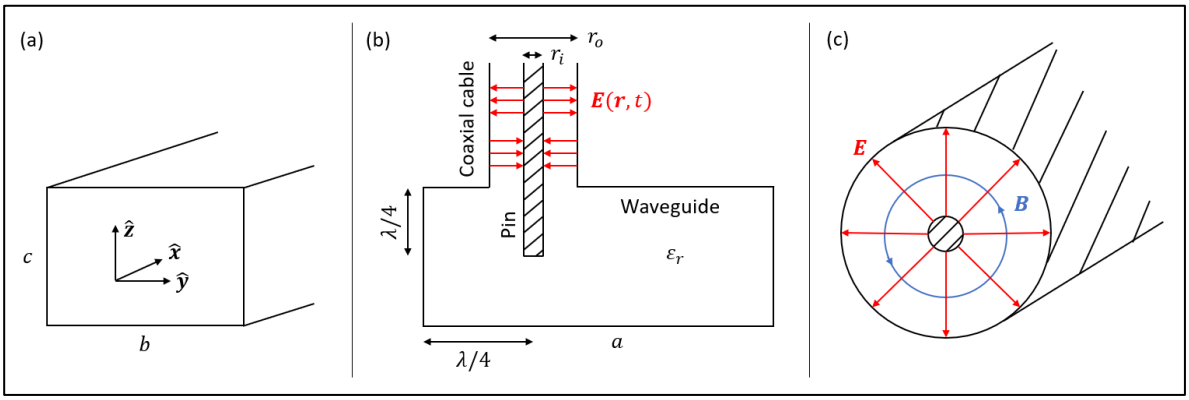

Fig. 1. (a) Waveguide cross-sectional area and Cartesian coordinate system. (b) Positioning of the antenna to excite EWs inside the rectangular waveguide (according to [21]). (c) Depicted TEM mode inside a coaxial cable (according to [19]).

2.3 Two-port signal detection

The VNA is responsible for signal generation and acquisition. With two connections for coaxial cables, it forms a two-port with which EWs can be excited inside and decoupled from the waveguide. Let i_1 and i_2 be the time-dependent input signals at port 1 and port 2 respectively and o_1 and o_2 the time-dependent output signals. The scattering matrix (also called S-matrix) consists of the relevant S-parameters S_{11}, S_{12}, S_{21} and S_{22}, which are determined by the following system of equations:

$$\begin{pmatrix} o_1 \\ o_2 \end{pmatrix} = \begin{pmatrix} S_{11} & S_{12} \\ S_{21} & S_{22} \end{pmatrix} \begin{pmatrix} i_1 \\ i_2 \end{pmatrix}. \tag{5}$$

The first index of S corresponds to the number of the output port and the second index to the number of the input port [19]. The output signals are often also specified as a matrix:

$$\begin{pmatrix} o_{11} & o_{12} \\ o_{21} & o_{22} \end{pmatrix} = \begin{pmatrix} S_{11}i_1 & S_{12}i_2 \\ S_{21}i_1 & S_{22}i_2 \end{pmatrix}. \tag{6}$$

The S-parameters are therefore quotients of the output and input signals. To transform from time to frequency domain, a Fourier transformation is performed according to [21]:

$$\tilde{S}_{ij}(f) = \frac{1}{\sqrt{2\pi}} \int_{-\infty}^{\infty} S_{ij}(t)\, e^{-2\pi i f t}\, dt. \tag{7}$$

In the exponent, i is the complex number.

2.4 Damage identification techniques

In many SHM applications, recorded digital signals S_{dam} of a damaged structure are compared with a reference S_{ref}. The reference consists of recorded signals from the previously intact structure. For better statistics, the reference signals are averaged in advance, provided that the frequency vectors are the same. Two methods, that are also common in impedance-based SHM procedures, are the RMSD and CCD. Both methods are based on different approaches but should lead to the same result of reliably detecting damages. For this purpose, DI are calculated to distinguish different structural conditions from each other.

The RMSD method is an additive method because a signal is subtracted from the reference at equal frequency bins. Finally, the RMS is calculated over all frequency bins. The following equation summarizes the calculation of DIs according to the RMSD:

$$\mathrm{DI}_{\mathrm{RMSD}} = \sqrt{\frac{1}{N}\sum_{i=1}^{N}(S_{\mathrm{dam}}[f_i] - S_{\mathrm{ref}}[f_i])^2}\,. \tag{8}$$

The CCD method is a multiplicative method in which the standard normal distributions of a signal and the reference are multiplied and summed afterwards over all frequency bins. The property of a standard normal distribution is the normalization of a signal to the expected value equal to 0 and the standard deviation equal to 1. Correlation coefficients therefore indicate in the value range $[0,1]$ how well one signal matches to the other. A correlation coefficient of 1 indicates identical signals and 0 indicates signals that are as different as possible. As a DI of 0 should not indicate any damage when the reference is compared with itself, the complement of the correlation coefficients must be considered as damage metrics. The correlation coefficients form a matrix, whereby the main diagonal elements result in 1 due to identical signals and the secondary diagonal elements are equal due to the commutative law. For this reason, it is sufficient for the symmetrical matrix to consider only one secondary diagonal element for damage diagnostics:

$$\mathrm{DI}_{\mathrm{CCD}} = 1 - \frac{1}{N-1}\sum_{i=1}^{N}\left(\frac{S_{\mathrm{dam}}[f_i] - \mu_{S_{\mathrm{dam}}}}{\sigma_{S_{\mathrm{dam}}}}\right)\left(\frac{S_{\mathrm{ref}}[f_i] - \mu_{S_{\mathrm{ref}}}}{\sigma_{S_{\mathrm{ref}}}}\right), \tag{9}$$

where, in general, μ_S is the expectation value and σ_S the standard deviation of S [22]. Optionally, all correlation coefficients can be combined by calculating the root mean square (RMS).

For a two-port, both reflection (back to the actuating antenna) and transmission parameters should be taken into account in a combined DI to make a more precise statement about the presence of damage. To ensure that all DIs have the same range, they are first normalized equal to 1. RMSD and CCD are considered separately, as both algorithms have different ratios in the DI of the structural states. For the combined DIs, the RMS is calculated using the individual DIs of all four S-parameters:

$$\mathrm{DI}_{\mathrm{comb,\,RMSD/CCD}} = \sqrt{\frac{1}{4}\sum_{i,j}\left(\frac{\mathrm{DI}_{\mathrm{RMSD/CCD}}(S_{ij})}{\max\left(\mathrm{DI}_{\mathrm{RMSD/CCD}}(S)\right)}\right)^2}. \tag{10}$$

3. Conception of a dielectric waveguide

3.1 Physical properties

Due to the metallic properties of an aluminum test plate, it is worth to design a DW for damage detection, which only needs to be placed over the device under test (DUT) to form metallic boundary conditions. Guided EWs can propagate in such a way that it is possible to change the scattering behavior of a generated damage. PP was chosen as dielectric due to its low cost and low absorption. According to the literature, the permittivity is 2.3 and the dielectric loss tangent below 0.001 at 36GHz [23]. Aluminum was also chosen for the metal walls.

A substrate made of PP with a monitoring area of $200\mathrm{mm} \times 100\mathrm{mm}$ was selected for a broad damage diagnosis. The thickness of the aluminum walls are 5mm at the edges and 3mm at the cover, according to the possibilities of the mechanical workshop. The DUT has a thickness of 10mm. Seven screws can be unscrewed with four different Allen keys to create a hole (here considered as reference damage).

The DW is operated from 20 to 40GHz. The challenge is to select the thickness of the substrate in such a way that only one relevant mode is generated at the central frequency of 30GHz. For the TE_{101} mode, equation (2) must be converted to c, resulting in a thickness of 3.30mm.

Equation (3) is used to check whether the skin effect becomes important in the frequency bandwidth at the aluminum walls with a conductivity of $3.56 \cdot 10^7\mathrm{S/m}$ (value is taken from CST Microwave Studio). This results in skin depths of $4.22 \cdot 10^{-7}\mathrm{m}$ up to $5.96 \cdot 10^{-7}\mathrm{m}$. The skin effect can therefore be neglected for thicknesses of 3mm to 10mm.

Finally, the correct type of connector has to be selected. The highest frequency for damage detection should be 40GHz. A suitable connector is the K-connector, which can usually operate up to 46.5GHz [24] without exciting interfering TE and TM modes in addition to TEM modes. The selected connector from *Pasternack* (product ID: PE45598) has an inner conductor diameter of 1.1684mm and an inner diameter of the outer conductor of 2.92mm. The dielectric is air, so that an upper limiting frequency of 46.67GHz is calculated using equation (4). Inside the connector, the inner conductor and dielectric taper to the pin, which has a diameter of 0.23mm.

3.2 Numerical modeling

The numerical modeling and simulation of the DW was carried out in CST Microwave Studio. The manufacturing possibilities of the mechanical workshop were already taken into account. The ports are defined rectangularly on the dielectric of the connector and the simulations are carried out with the time domain solver. The numerically calculated input and output signals are shown in Fig. 2 in time domain and in Fig. 3 in frequency domain for an undamaged aluminum DUT.

The input signal at both ports is a narrow chirp. It has the option to propagate in the DW to the opposite port or to be detected as a reflection signal. A peak can already be seen in the reflection signals after approximately 0.1ns, which means that EWs have already been partially reflected inside the connector back to the applied port. Further reflections can be explained by the scattering in the DW, which become relevant after 2.1ns. This is the time it takes for an EW to propagate from one port to the opposite end of the DW and back again ($2 \times 200\text{mm}$). Therefore, the first transmission signal is detected at the opposite port in the half time. Further peaks can be seen in o_{12} and o_{21}, which are detected one by one depending on the group delay of the EWs. In contrast to the phase velocity, the group velocity increases with increasing frequency. According to the law for unaccelerated movements, the group delay decreases with increasing group velocity for the same covered distance [6].

The frequencies that ensure increased transmission of EWs in the DW can be seen in the S_{11} and S_{22} parameters in shape of dips. The wide, deep dip around the center frequency of 30GHz was achieved. Due to the symmetry of the DW, the reflection parameters S_{11} and S_{22} and the transmission parameters S_{12} and S_{21} are almost identical. There are small deviations in the reflection parameters because the holes of the DUT are arranged asymmetrically and the modeled screw does not close the entire hole in the reference state.

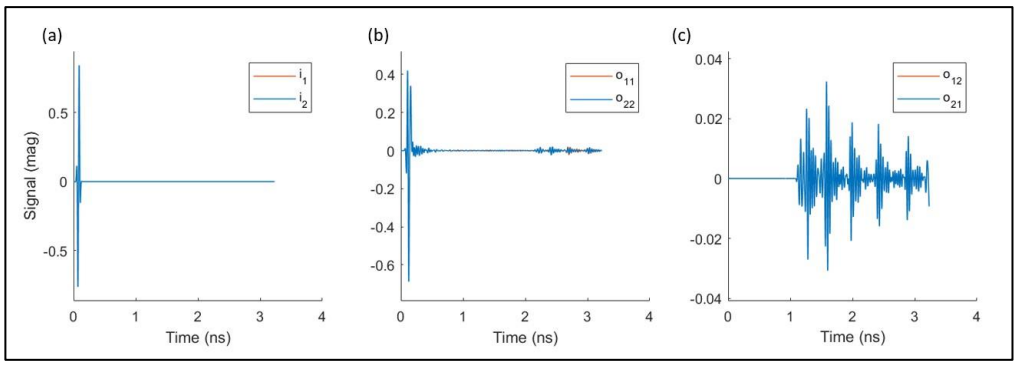

Fig. 2. Simulated (a) input, (b) reflection and (c) transmission signals of the reference state in time domain.

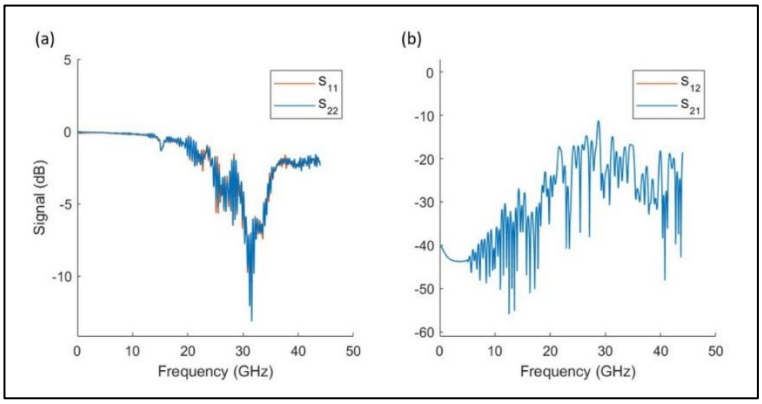

Fig. 3. Simulated (a) reflection and (b) transmission signals of the reference state in frequency domain.

3.3 Experimental setup

The DW was manufactured for laboratory purposes using the simulation model. This is shown in Fig. 4(a). The coaxial cables are screwed to the connectors and thus connect the DW with the M9807A PXI VNA from *Keysight*. The manufacturer's *NetworkAnalyzer* software enables calibrating the used coaxial cables and triggering a measurement. The frequency bandwidth and the number of sampling points can be set. The maximum bandwidth of 0.01MHz up to 44GHz was used, whereby the damage diagnosis was only carried out from 20GHz to 40GHz. The number of sampling points was limited to 1001, as CST also always generates 1001 sampling points for the S-parameters. Only the S-parameters are plotted on the user interface of the *NetworkAnalyzer* software, which can also be saved as s2p files.

Fig. 4(b) shows the arrangement of the unscrewable Allen screws of the DUT to create a hole that represents a structural damaged state. The positions of the connectors are also outlined in the figure. The measurement plan was designed in such a way that ten measurements per structural condition were triggered manually for better statistics. Starting with the reference state, the following screws are removed one by one in order of increasing diameter: #1 (2mm), #2 (4mm), #3 (4mm), #4 (6mm), #5 (8mm), #6 (8mm) and finally #7 (8mm). At the end of this section, the entire setup, including the measurement and evaluation process, is shown schematically in Fig. 5.

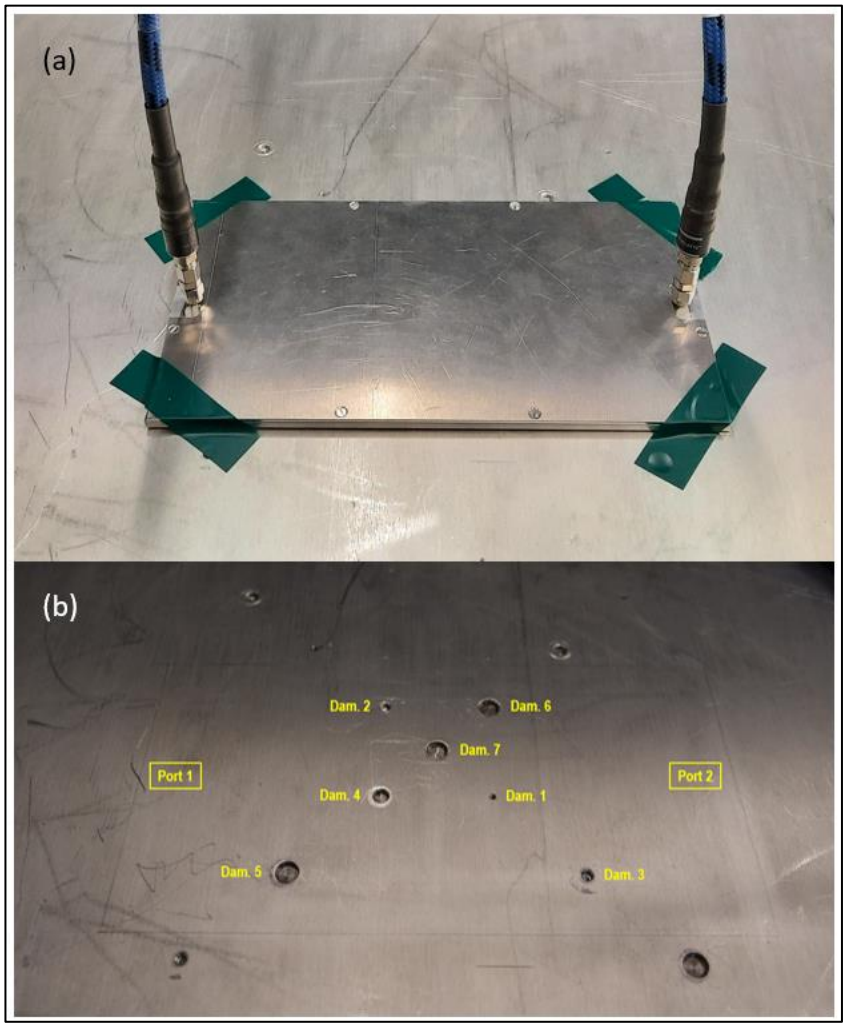

Fig. 4. (a) Setup in the lab. The DW is fixed at the DUT with tape. The coaxial cables are routed from the VNA to the DW. (b) Unscrewable screws (numbered) in the DUT.

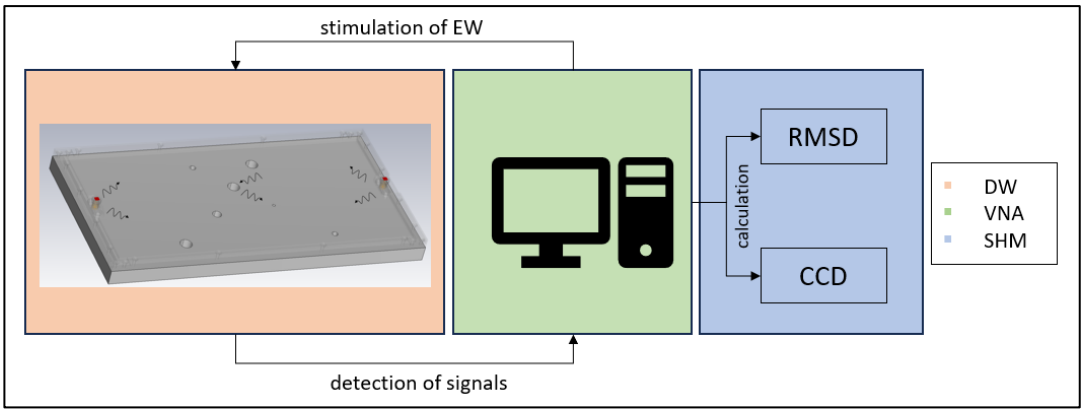

Fig. 5. Schematic representation of the measurement and evaluation process.

4. Experimental results

Due to symmetrical conditions in the DW, only the S_{12}- and S_{22}-parameters are shown in Fig. 6 and discussed below. Ten measurements per structural state have already been averaged in order to limit the number of plots in a graph.

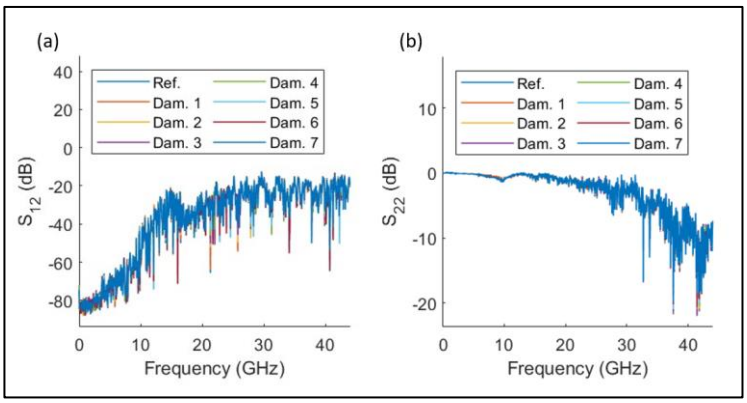

Fig. 6. Trends of the experimentally measured and averaged S_{12}- and S_{22}-parameters.

It is noticeable that the signals are noisier than those from the simulation. One reason for this are the imperfect metallic boundary conditions due to the simple gluing of the waveguide to the DUT. It can be assumed that there are gaps through which EWs escape from the DW and the signal energy consequently decreases.

Another observation are the different trends compared to the simulation results in Fig. 3. Beyond 30GHz, there are further dips that are even deeper. Possible reasons for this are the small bending of the substrate caused by the manufacturing process and artifacts of the VNA and especially of the coaxial cable. As soon as the coaxial cable is touched, noticeable significant changes in the S-parameters are already recognizable.

The curves look similar for all structural states. The changes, that are relevant for damage diagnosis, are small. Since the DIs, calculated by the RMSD and CCD method after equation (8) and (9) respectively, are similar, only the normalized DIs after the RMSD for S_{12} and S_{22} are shown in Fig. 7. The individual reference states as well as the damaged states are compared with the averaged reference in order to evaluate the deviations of the signals within a structural state. In relation to the DIs of the damaged states, those of the reference state are small.

Fig. 8 shows the combined and normalized DIs calculated by equation (10). An unambiguous trend can be observed: As soon as the severity increases with the increasing number of holes, the DIs also increase. Due to mean signals, the DI of the reference state is

zero due to the difference value formation in the RMSD and the calculation of the correlation coefficients in the CCD. Although holes with larger diameters are more clearly delineated, damage identification of holes with all diameters from 2mm to 8mm is still possible.

Physically, the signal changes with each structural state can be explained by the fact that, on the one hand, EWs emerge from the DW through the holes. Depending on the diameter, the drop in signal amplitude is frequency-dependent. On the other hand, the interruption of the barrier-free propagation of EWs causes a discontinuity in the current distribution on the inner surface of the metal walls. Scattering effects become more important.

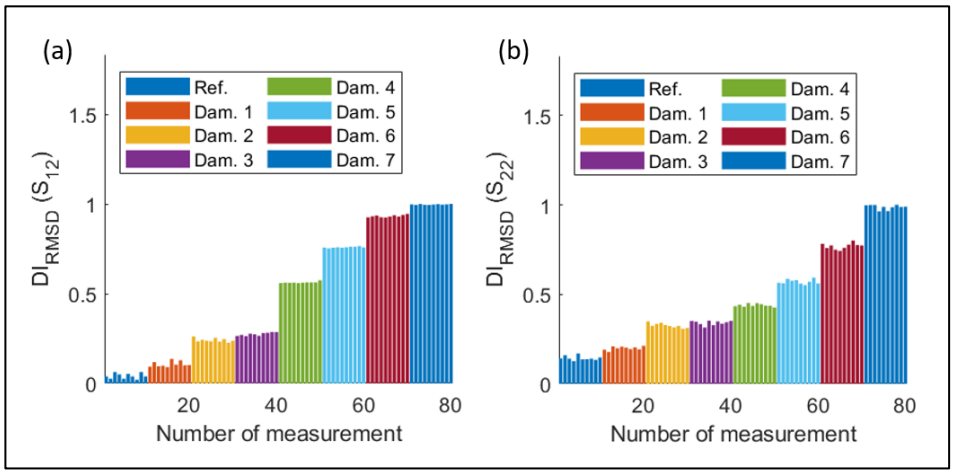

Fig. 7. Normalized DI, calculated by the RMSD method for S_{12} and S_{22}.

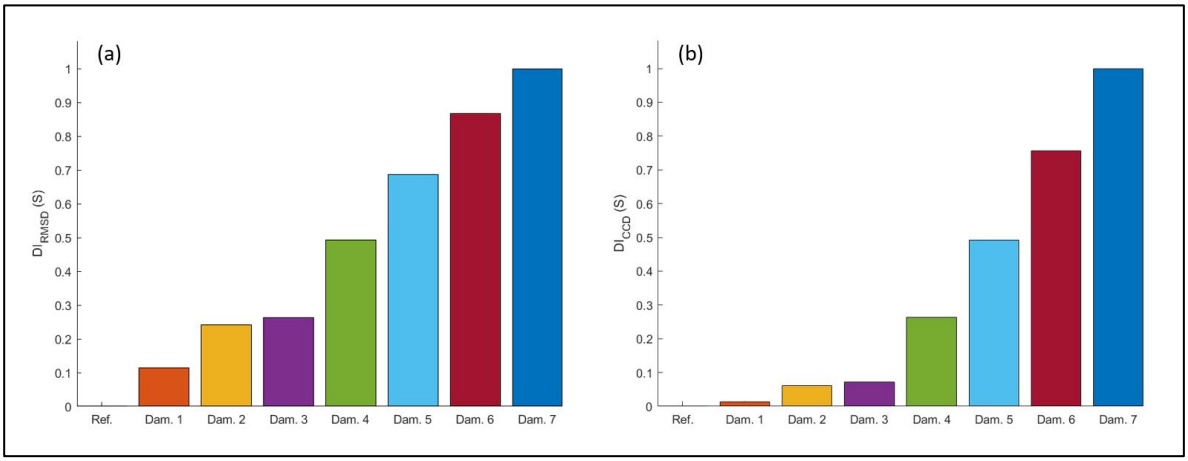

Fig. 8. Combined and normalized DI, calculated by the (a) RMSD and (b) CCD method.

5. Conclusions

In this paper it was shown that damage detection of holes in an aluminum DUT down to a diameter of 2mm is possible using guided EWs. The centerpiece of this work is the rectangular DW, which was specially designed for operating in the K_a-band. The RMSD and CCD were used as algorithms for SHM. The resulting DIs, obtained from the S-parameters of a two-port, were combined into one DI to consider reflection and transmission ratios equally. The result was an increase in the DIs with an increasing number of generated holes.

The developed DW can be used for the SHM of aerospace structures. An optimization for the fixation of the DW to a DUT would be the use of screws instead of tape for better metallic boundary conditions. Furthermore, local SHM algorithms are advantageous to detect the position of damage for maintenance in advance.

Acknowledgement

The authors gratefully acknowledge the financial support of this research by the Federal Ministry for Economic Affairs and Energy (Grant Number: 20Q1911C).

References

[1] Alanazi, M.D.: A Review of Dielectric Resonator Antenna at Mm-Wave Band. Eng. 4(1), 843-856 (2023).
[2] Mongia, R.K.; Ittipiboon, A.: Theoretical and Experimental Investigations on Rectangular Dielectric Resonator Antennas. IEEE Transactions on Antennas and Propagation. 45(9), 1348-1356 (1997).
[3] Abbas, Z; Pollard, R.D.; Kelsall, R.W: Complex permittivity measurements at Ka-Band using rectangular dielectric waveguide. IEEE Transactions on Instrumentation and Measurement. 50(5), 1334-1342 (2001).
[4] Memmolo, V.; Moll, J.; Nguyen, D.H.; Krozer, V.; Holstein, J.; Kapoor, R.; Stindl, J.: Assessment of Damage in Metallic Plates by Ultra-Wideband Guided Electromagnetic Waves. 48th Annual Review of Progress in Quantitative Nondestructive Evaluation (2021).
[5] Memmolo, V.; Fox, L.; Moll, J.; Krozer, V.: Structural Health Monitoring of Metallic Tubes inducing Guided Electromagnetic Waves. 17th European Conference on Antennas and Propagation (2023).
[6] Rao, M.E.; Maetz, T.; Moll, J.: Numerical Analysis of Dispersion Compensation for Guided Electromagnetic Waves in Rectangular Microwave Waveguides. 16th European Conference on Antennas and Propagation (2022).
[7] Moll, J.; Nguyen, D.H.; Krozer, V.: Guided Electromagnetic Waves for Damage Localization in a Structural Health Monitoring Framework. European Workshop on Structural Health Monitoring (2020).
[8] Memmolo, V.; Moll, J.; Bonet, M.M.; Schmidt, D.; Krozer, V.: Ultra-wideband microwave leakage monitoring for stringer debonding detection in carbon composite fuselage structures. NDT & E International. 142 (2023).
[9] Mikhnev, V.; Stelmaszczyk, K.; Knap, W.: Optimization of the Dielectric Waveguide Sensor Using Analysis of Confinement of the Guided Wave. 24th International Microwave and Radar Conference (2022).
[10] Shibata, T.; Hashizume, H.; Kitajima, S.; Ogura, K.: Experimental study on NDT method using electromagnetic waves. Journal of Materials Processing Technology. 161(1-2), 348-352 (2005).
[11] Baer, C.; Fernandez, J; Musch, T.: A Dielectric Waveguide based Signal Distribution Network for Time Multiplexed Fixed Target Radar Measurements. 18th European Radar Conference (2021).
[12] Koala, R.; Maru, R; Iyoda, K.; Yi, L.; Fujita, M.; Nagatsuma, T.: Ultra-Low-Loss and Broadband All-Silicon Dielectric Waveguides for WR-1 Band (0.75–1.1 THz) Modules. Photonics. 9(8), 515 (2022).
[13] Bauer, M.; Matheis, C.; Mashkin, A.; Krane, S.; Pohlmann, F.; Friederich, F.: Terahertz Non-destructive Testing of the Mica Insulation of Power Generator Bars in FMCW Measurements with a Dielectric Waveguide Antenna. 51st European Microwave Conference (2021).
[14] Weinzierl, J.; Richter, J.; Rehm, G.; Brand, H.: Simulation and Measurement of Dielectric Antennas at 150 GHz. 29th European Microwave Conference (1999).
[15] Galler, T.; Hügler, P.; Chaloun, T.; Waldschmidt, C.: Dielectric Rod Antenna for Glass-Packaged Radar Sensors at G-band. 14th German Microwave Conference (2022).
[16] Geiger, M.; Hitzler, M.; Iberle, J.; Waldschmidt, C.: A dielectric lens antenna fed by a flexible dielectric waveguide at 160 GHz. 11th European Conference on Antennas and Propagation (2017).
[17] Geiger, M.; Hitzler, M.; Waldschmidt, C.: Mechanically Decoupled Transitions from MMIC to Rectangular and Dielectric Waveguides at G-Band. IEEE/MTT-S International Microwave Symposium (2020).
[18] Lin, I.K.C.; Jamaluddin, M.H.; Gaya, A.: A Triple Band Substrate Integrated Waveguide with Dielectric Resonator Antenna for 4G and 5G Applications. Micromachines. 14(7), 1284 (2023).
[19] Pozar, D.M.: Microwave Engineering. Wiley, New York City, 4th ed. (2012).
[20] Basavarajappa, G; Mansour, R.R.: A High-Q Quadruple-Mode Rectangular Waveguide Resonator. IEEE Microwave and Wireless Components Letters. 29(5), 324-326 (2019).
[21] Heuermann, H.: Mikrowellentechnik. Springer Vieweg, Wiesbaden (2020).
[22] Min, J.; Park, S.; Yun, C.-B.; Lee, C.-G.; Lee, C.: Impedance-based structural health monitoring incorporating neural network technique for identification of damage type and severity. Engineering Structures. 39, 210-220 (2012).
[23] Yao, H.-Y.; Hsiao, D.-R.; Chang, T.-H.: Fast, Nondestructive, and Broadband Dielectric Characterization for Polymer Sheets. Polymers. 12(9), 1891 (2020).
[24] Skinner, D.: Guidance on using precision coaxial connectors in measurement. NPL guide, 3rd ed. (2007).